Imperfect focal conic domains in A smectics: a textural analysis

Yu. A. Nastishin[abc]; C. Meyer[a]; M. Kleman[b]

[a] Physique des Systèmes Complexes, Université de Picardie, 80039 Amiens, France [b] Institut de Minéralogie et de Physique des Milieux Condensés, CNRS UMR 7590, Université Pierre-et-Marie-Curie, Campus Boucicaut, 75015 Paris, France [c] Institute for Physical Optics, Lviv 79005, Ukraine

PLEASE SCROLL DOWN FOR ARTICLE

Taylor & Francis
Taylor & Francis Group

Imperfect focal conic domains in A smectics: a textural analysis

Yu. A. Nastishin[abc]*, C. Meyer[a] and M. Kleman[b]

[a]*Physique des Systèmes Complexes, Université de Picardie, 33 rue Saint-Leu, 80039 Amiens, France;* [b]*Institut de Minéralogie et de Physique des Milieux Condensés, CNRS UMR 7590, Université Pierre-et-Marie-Curie, Campus Boucicaut, 140 rue de Lourmel, 75015 Paris, France;* [c]*Institute for Physical Optics, 23 Dragomanov Street, Lviv 79005, Ukraine*

We have analysed optical microscopy observations of focal conic domains (FCDs) with imperfect ellipses on the basis of the theoretical concepts developed by Kleman et al. (*Philos. Mag.* **2006**, *86*, 4439). Two types of imperfect ellipses are observed: with *kinks* (elementary imperfections resulting from a topological interaction of a disclination with a dislocation, at their point of junction) being either in the ellipse plane ('mouse') or perpendicular to it ('turtle'). The experimental conditions for the observation of imperfect FCDs of both types are described. A model describing the shape of a mouse-type ellipse is compared with observations. Two experimental observations in *nematogenic* smectics (i.e. which have a smectic → nematic transition) emphasise the predominant role of kinks in dynamical phenomena involving dislocations and FCDs: (i) a reversible and sudden temperature-induced transformation between two FCD textures, i.e. FCDs with fewer kink-carrying distortions (called isometric textures) and the higher temperature FCDs with a proliferation of kinks (called non-isometric); (ii) a shrinking of the ellipses upon heating, up to their sudden and total disappearance at a temperature well below the phase transition. In contrast, in a *non-nematogenic* smectic, the ellipse size does not vary upon heating until the appearance of the isotropic phase.

Keywords: Smetic A; defects; imperfect focal conic domains; dislocations

1. Introduction

Topological line defects are well known in crystalline solids; the standard example is *quantised dislocations* (*1*), which break translational symmetries. Quantised dislocations are also present in liquid crystals (LCs) with quantised translation symmetries, for example, in layered media such as smectic phases (*2, 3*), the defects of which are described in this paper.

As in all liquid crystalline phases, smectics also display another type of topological line defect, *disclinations* (*4, 5*), which break rotational symmetries. Disclinations in layered media have specific properties. Whereas disclinations in LCs with *continuous* translation symmetries (e.g. nematics) can take any shape, they are well geometrically defined in smectic A (SmA) phases, where they most often appear as paired conics, namely an ellipse and a hyperbola in a conjugate relationship, which delimit a *focal conic domain* (FCD) inside which the layers are parallel. The ellipse and the hyperbola are focal lines of this set of layers, see (*5, 6*) for details. This special disclination geometry is related to the fact that the curvature deformations of the layers are much less costly than strain deformations. This also means that plastic deformations tend to relax with as few dislocations as possible.

The presence of dislocations in interaction with disclinations is of course unavoidable in a plastically deformed medium; the interaction between a disclination conic and a dislocation shows up specific features when they are in *contact*, which results in a local distortion of the conic away from its ideal elliptic or hyperbolic shape, at the location where the two defects meet. Such local distortions are called *kinks*. They have been recently reported in smectic phases (SmA) of various LC materials (*7, 8*). The empirical observations enable us to distinguish between those kinks that are observable with light microscopy (*macroscopic kinks*) and those that are not (*microscopic kinks*). An *isolated* microscopic kink implies the interaction of a microscopic Burgers vector dislocation with the disclination; a *density* of microscopic kinks affects the shape of the disclination with which the dislocations interact (what we loosely call an *imperfect* conic, in contrast with an *ideal* conic); a *macroscopic* kink is the result of the interaction of a macroscopic Burgers vector dislocation with a disclination, or of the accumulation at neighbouring locations on a disclination of microscopic Burgers vector dislocations of the same sign.

In the remainder of this introduction we recall the essential topological properties of a kink.

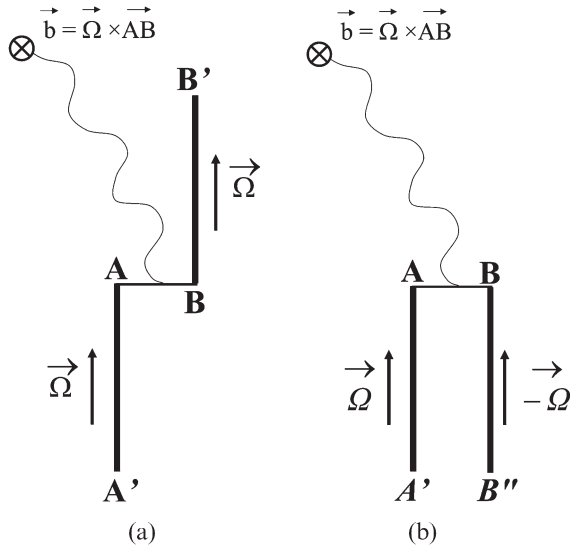*Corresponding author. Email: nastyshyn_yuriy@yahoo.com

Figure 1. Distorted wedge disclination line $A'B'$ of a rotation vector $\vec{\Omega}$: (a) attachment of a dislocation (shown by a thin wavy line) of Burgers vector $\vec{b}$ to the disclination results in the presence of a kink AB connecting two half infinite segments, AA' and BB' of the disclination; (b) the segment BB' transformed into the segment BB'' carrying the opposite rotation vector $-\vec{\Omega}$, by continuous transport.

The concept of kink is very general; it is valid for all dislocation–disclination interactions, in smectics as well as in nematics and other media where the concepts of dislocation and disclination make sense altogether, when defects are merging (*9, 10*). The principle of the interaction is sketched in Figure 1 and can be summarised as follows.

Consider a disclination line made of two half infinite wedge segments, $A'A$, BB' linked by a segment AB of twist character, a kink on the disclination $A'B'$, Figure 1 (a). We recall that a *wedge* disclination line segment is a line segment parallel to the rotation vector, here denoted by $\vec{\Omega}$; a *twist* disclination line segment is perpendicular to the rotation vector $\vec{\Omega}$. This geometry is equivalent to the geometry of Figure 1 (b), where the segment BB' has been 'smoothly' transported to the position BB'' and its orientation reversed, so that it can now be considered as carrying the rotation vector $-\vec{\Omega}$. The segments $A'A$ and BB'' are wedge disclination segments of opposite rotations and thereby carry together a translation

$$\vec{b} = \vec{\Omega} \times \overrightarrow{AB}. \tag{1}$$

Together, they are therefore equivalent to a dislocation of Burgers vector $\vec{b}$. Thus, because of the law of conservation of the Burgers vector, a dislocation of Burgers vector $\vec{b}$ is attached to AB in Figure 1 (b).

Transporting back BB'' to BB', it appears that a dislocation with the same Burgers vector $\vec{b}$ is attached to the kink AB in Figure 1 (a). The Burgers vector $\vec{b}$ has to be a translational symmetry of the medium under consideration, i.e. in a smectic a multiple of the layer thickness d_0. However, the reasoning applies to any medium, for example, the nematic liquid crystalline phase, where translational symmetries are not quantised: in that case the curved continuous shape of a disclination can be analysed in terms of densities of *continuous dislocations*, and the flexibility and the mobility of disclinations in nematics can be analysed in processes of annihilation and creation of such dislocation densities.

We have already made a distinction between macroscopic and microscopic kinks. Another useful distinction directly related to the present paper is between two types of kinks, namely kinks in the ellipse plane (first type) and kinks perpendicular to the ellipse plane (second type). According to equation (1), the Burgers vectors of the attached dislocations are either perpendicular to a direction belonging to the plane of the ellipse or of the hyperbola (first type), or parallel to the plane of the ellipse or of the hyperbola (second type). In either case, the Burgers vectors, which are along the translation symmetry directions, have to be either perpendicular to the smectic layers, if the broken translations are quantised ($b=nd_0$), or parallel to the layers, if the broken translations are continuous. Here we are only interested in *quantised* dislocations (see (*10*) for a discussion of *continuous* dislocations in smectics). According to this analysis, the orientation of the layers with respect to the plane of the conic is thereby an important element in classifying the types of dislocations attached to a kink.

Layers *inside* a FCD are perpendicular to the plane of the ellipse in its vicinity; therefore dislocations in this region are preferentially attached to kinks of the second type on the ellipse. Likewise, dislocations outside the FCD are preferentially attached to parallel kinks of the first type. Similar remarks can be made, *mutatis mutandis*, for hyperbolae. In fact, all of the observations reported in the following are regarding imperfect ellipses. We have not made a comparable systematic study of kinks on hyperbolae; see (*11*) for one relevant observation.

It is important to observe that the foregoing considerations do not appeal at all to the principles of the topological theory of defects, but to the more ancient Volterra process, suitably extended. We refer the reader to (*10*) for a full discussion of this topic.

2. Experimental results

2.1. *Materials, sample preparations*

The smectic materials studied in this paper belong to the cyano- and cyano-oxy-biphenyl series; they were purchased from Merck. 8CB, 8OCB and 9CB exhibit a nematic phase above the SmA phase (*nematogenic* materials), whereas 10CB transits directly from the SmA phase into the isotropic phase (*non-nematogenic* material). The temperature control is performed using a Hot Stage HS-2 from Instec which provides a thermo-stabilisation accuracy of $\pm 0.002^{\circ}$C and a temperature change at a controlled rate, which can be as low as 0.001°C min^{-1}.

Reviewing the literature on FCDs in smectics we find that in most papers the FCDs are studied as they appear per chance in a sample. An FCD texture appears spontaneously either after melting from the crystalline state or on cooling from a higher temperature phase in a sample between two untreated glass substrates (*6, 12–14*). Although it is not difficult to obtain the FCD texture, the preparation of a FCD with desired predicted geometrical characteristics is not an easy task. Moreover, in practice it appears difficult to pick up a FCD satisfying the experimental requirements (desired and controllable eccentricity, size and orientation of the ellipse and hyperbola) from the real FCD texture. In real samples the examination of the FCD belonging to a texture is complicated by other accompanying defects: other FCDs, curvature walls, clusters of dislocations including those with giant Burgers vector and other smectic distortions. In the following sections we consider three different experimental geometries for the preparation of the FCDs, namely: (i) free-standing films, (ii) hybrid aligned films with special types of anchoring conditions, (iii) films between untreated clean glass substrates, separated by spacers of thickness 200 μm. These geometries induce different types of FCD textures.

The first two methods of preparation, namely free-standing films and films deposited on a solid substrate, produce FCDs with ellipses that are roughly parallel to the microscope view field. The third method of preparation allows observation of the FCDs from the side. A gentle heating of the solid material above the crystal–SmA transition allows us to find many FCDs located deeply in the bulk of the SmA sample with their ellipses significantly tilted with respect to the microscope field view. We call such FCDs *lopsided*.

Experimentally, we observes two types of imperfect ellipses (*7, 8*), which we call, in accordance with the shapes they take, the *mouse* (in free-standing films; a mouse carries a large density of kinks of the first type), and the *turtle* (in hybrid films spread on a substrate with quasi-planar anchoring and in thick cells; a turtle carries a large density of kinks of the second type). Kinks on a turtle are often macroscopic. Imperfections of both types can also coexist on the same ellipse. In the third type of samples, the *lopsided* ellipses (and the FCDs they carry), which are seemingly ideal, display a remarkable temperature evolution, most conspicuously close to the nematic transition; no doubt this evolution is related to dynamical kinks. More generally, kinks should play a role in the size transformations and mobility of ideal FCDs.

More details about the characteristics of the various types of samples are given below.

2.2. *Macroscopic kinks*

Within this section we deal with hybrid aligned SmA (8CB) films spread on glass substrates treated for planar alignment of the director. The second film interface is in contact with air where molecular anchoring is homeotropic. Two types of glass substrate have been used. The substrates of the first type have been rubbed several times unidirectionally with a Kimwipes napkin (from Kimberly-Clark) wetted in glycerol (wet-glycerol rubbing) and the others have been spin-coated with a polymer (PI 2555) layer unidirectionally rubbed with velvet (dry rubbing). The LC material is then spread over with a blade along the rubbing direction. By rubbing a clean glass substrate with a napkin wetted in glycerol, we expect that the azimuthal anchoring strength will be weaker than it is for the dry rubbing of the polymer layer. In both cases we find FCDs. The difference is that for the dry rubbing the kinked FCDs of equal size are tightly packed in a quasi-hexagonal lattice (Figure 2), while for the wet-glycerol rubbing we find a polygonal texture containing very large turtle kinked FCDs. We do not discuss the origin of these textural differences, but retain the empirical conclusion that the wet-glycerol rubbing is helpful for the preparation of the turtle kinked FCDs. Hybrid director orientation favours the appearance of the FCDs but the presence of a particular direction of the easy axis at the solid interface conflicts with the star-like geometry of the director field within the FCD in the ellipse plane. This leads to the formation of large Burgers vector kinks on the ellipses, well observable under the optical microscope.

2.2.1. *SmA film on a wet-glycerol rubbed glass substrate: turtle textures*
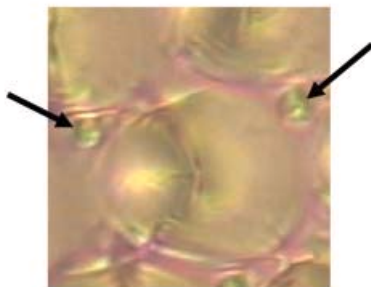
Assume that we have first hybrid anchoring conditions and zero pretilt at the substrate with planar alignment (the pretilt angle is the angle between the

$T-T_c = -0.6\ ^oC$

$-0.6\ ^oC < T-T_c < 0\ ^oC$
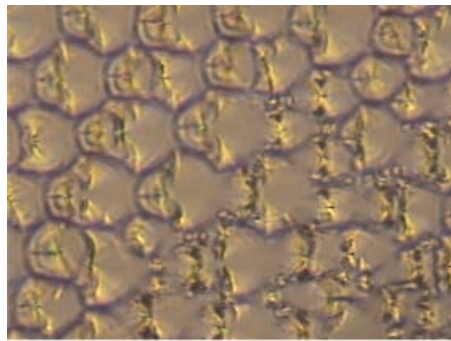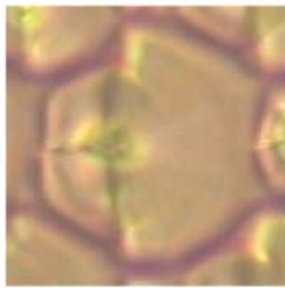
$T-T_c < -0.6\ ^oC$

Figure 2. Texture of the SmA film spread on the glass substrate covered by rubbed polyimid PI-2555 with a free second interface. (a) Demonstration of the textural change coming from the right lower corner at $T=T^*$. (b), (c) The same elementary domain of the texture above and below T^*, respectively. Here T^* is 0.6°C below the SmA–N transition.

director at the solid surface and this substrate); the ellipse is usually located on this planar substrate. The director then coincides with the easy axis only along one direction of the full set of the star-like directions of the director field. It is presumed that the major axis of the ellipse is oriented along the easy axis. For all other directions, the director deviates from the easy axis direction with the maximal deviation (of 90°) being along the direction passing through the ellipse focus parallel to the minor axis.
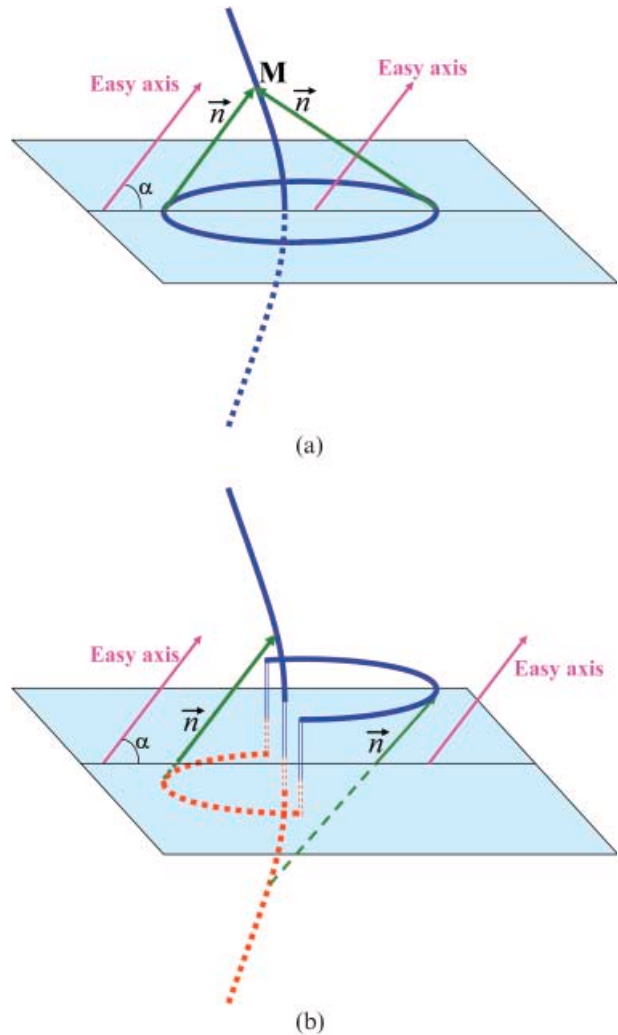

(a)

(b)

Figure 3. (a) At non-zero pretilt the director in the FCD is not aligned with the easy axis. (b) The conflict between the polar anchoring and the circular geometry of the director field in the FCD can be softened by introducing a double kink, perpendicular to the ellipse plane.

For non-zero pretilt of the director, the conflict between the star-like director field geometry within the ellipse and the unidirectional anchoring conditions is even more pronounced. For the ellipse located in the substrate plane, there is no direction along which the director can coincide with the easy axis. Setting the ellipse at some distance below or above the substrate (the distance depends on the value of the pretilt angle), we can satisfy the pretilt anchoring conditions along one of the radii emanating from the physical focus, whereas along the opposite radius, the director tilt required by the FCD geometry is parallel to the mirror image of the easy axis with respect to the substrate.

This is illustrated in Figure 3 (a) and (b). Let M be a point on the hyperbola; consider the cone C_M of
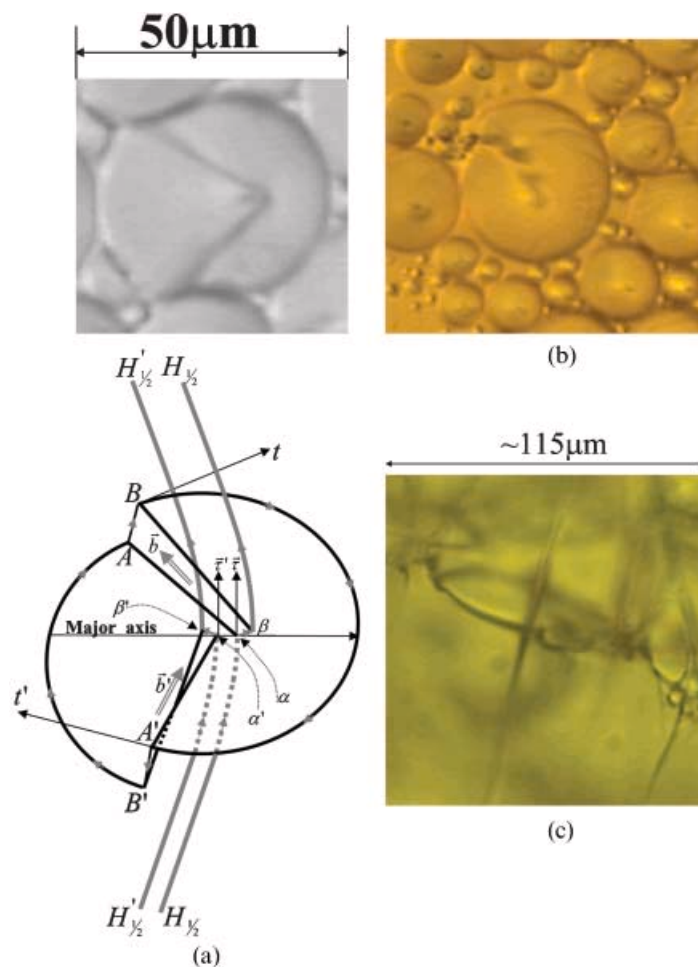
Figure 4. Imperfect FCDs of the turtle type: (a) symmetrically double kinked, see the text for details; (b) asymmetrically kinked, one of the two kinks is smoothly spread along the ellipse; (c) a lopsided kinked FCD of the turtle type observed in thick samples between untreated glass substrates.

apex *M* that leans on the ellipse (see Figure 3 (a)). Its generatrices are along the SmA molecular directions. The director can coincide with the easy axis (at an angle α in Figure 3) only on one side of the hyperbola along one side of the major axis, and is very different along the other side. The scheme in Figure 3 (b) demonstrates that the conflict between the non-zero director pretilt and the FCD construction can be weakened if the two parts of the FCD on both sides of the hyperbola are shifted with respect to each other along the substrate normal. Such an operation results in the presence of a double kink on the ellipse. The left part of the ellipse becomes virtual, as it is below the LC interface and the director appears parallel to the easy axis all along the major axis of the ellipse. A FCD of this type, namely a double kinked turtle, is shown in Figure 4 (a). The two parts of the double kinked ellipse are not at the same level: the kinks have a measurable vertical component of the order of a few micrometres. On the other hand there is a horizontal component (the kinks are oblique with respect to the ellipse plane) so that the two parts of the double kinked ellipse cannot be fitted together. We comment here only on the vertical component of the kink. Figure 4 (b) shows a turtle with one of the two kinks smoothly spread along the ellipse. Figure 4 (c) shows a lopsided kinked FCD of the turtle type observed in thick (200 µm) samples between untreated glass substrates. The steps which link the kinks on the ellipse to the hyperbola are most remarkable. They must be understood as sets of screw dislocations whose total Burgers vector $\vec{b}$ obey equation (1) on the ellipse and on the hyperbola.

In our observations shown in Figure 4 (a) the details of the attachment of the steps to the hyperbola are below the microscope resolution; we analyse the situation as follows. Let us assume (this is a thought experiment) that the hyperbola (which is a wedge disclination of strength $k=1$, i.e. it carries a 2π rotation) is split into two independent wedge

disclinations $H_{1/2}$ and $H'_{1/2}$ of the same hyperbolic shape, of strength $k=1/2$, i.e. each carrying a π rotation. We also assume that each step originating on a kink on the ellipse ($\overrightarrow{AB}$ or $\overrightarrow{A'B'}$) is attached to a kink on one of the hyperbolae (denoted by $\overrightarrow{\alpha\beta}$ and $\overrightarrow{\alpha'\beta'}$). We therefore have, according to equation (1),

$$\vec{b} \sim \vec{t} \times \overrightarrow{AB} = \vec{\tau} \times \overrightarrow{\alpha\beta}, \qquad (2)$$

and a similar equation for $\overrightarrow{A'B'}$ and $\overrightarrow{\alpha'\beta'}$. Here $\vec{t}$ (respectively, $\vec{\tau}$) is the unit tangent vector to the oriented ellipse (respectively, the hyperbola) at the kink locations: the rotation vectors are indeed tangent to the conics. In the sketch of Figure 4 (a), it is assumed that along the ellipse we have the sequence A, B, A', B', so that $\overrightarrow{AB} = -\overrightarrow{A'B'}$, and that the two $k=1/2$ hyperbolae are oriented parallel to one another. By symmetry, $\vec{\tau}$ is perpendicular to the ellipse plane, so that we expect $\overrightarrow{\alpha\beta}$ to be in the ellipse plane, in a simple model; thus the step joining $\overrightarrow{AB}$ and $\overrightarrow{\alpha\beta}$ should be twisted.

Now, the idealised sketch of Figure 4 (a) has to be modified to take the real situation into account. The essential difference comes from the fact that at some distance from the kinks $\overrightarrow{\alpha\beta}$ and $\alpha'\beta'$, on each side of the ellipse plane, the two $k=1/2$ hyperbola segments should merge into a unique $k=1$ hyperbola segment. In this operation, the kinks come near to one another and tend to align (which is observed, seemingly) implying they interact. In particular, we no longer expect the step dislocations to be of a screw character in the vicinity of the kinks. However, our analysis is only a first approximation, and has to be completed after more observations have been made.

2.2.2. SmA film on a glass substrate covered with rubbed PI-2555: a textural transformation

When deposited on a glass substrate and covered with a unidirectionally mechanically buffed polymer PI-2555, the investigated LC materials we have studied show quasi-planar alignment of the director with a pretilt angle of about $3°$ (see (15, 16)). The sample is heated to the nematic phase and slowly cooled down to the SmA phase. The texture of the SmA after cooling displays a quasi-hexagonal pattern of domains which, for similar geometry of the hybrid SmA between two solid substrates, have been proven elsewhere to be composed of fragmented FCDs with smectic layers carrying a negative Gaussian curvature (17).

The elementary units of the quasi-hexagonal pattern suffer from a *textural transformation* at a

temperature T^* approximately $0.6°C$ below the smectic–nematic transition. The transformation is evidenced in the upper photograph of Figure 2. The right lower corner displays the appearance of a new texture. The arrows in the lower photograph of Figure 2 point to small FCDs that have appeared for $T<T^*$. In contrast, at $T>T^*$ the interstices between the domains are free of any visible defects and, thus, according to the model of Kleman and Lavrentovich for a tilt grain boundary in a smectic (see Appendix A for a short introduction and (18) for details) are full of optically invisible elementary dislocations, replaced below T^* by the small FCDs just alluded to. (These FCDs and elementary dislocation sets are topologically equivalent in the sense that they yield the same orientation of the director at a distance from the plane of the ellipse (18). See (19) for probably the first observation of this equivalence, with FCD ellipses and dislocations located at the substrate.) The middle and lower photographs in Figure 2 show the textures of the same elementary domain above and below T^*, respectively. Our opinion is that the texture in Figure 2 corresponding to $T>T^*$ (middle photograph) represents a double kinked FCD, presumably of the Mouse type, with the in-plane kinks connecting arcs of two co-focal ellipses with different diameters. This result follows from the fact that the size of the ellipse fragment in the right part of the FCD is much larger than in the left part. The reason for such a construction could be that the left part of the FCD, where the smectic layers are strongly curved and hence strongly conflicting with the unidirectional anchoring, is limited by the arc belonging to an ellipse of smaller size, and the other (right) part, where the layers are less curved, is limited by the arc of the larger size ellipse. The observations show that on cooling at $T=T^*$ the kinks shorten. Shortening of the kink is in agreement with the decrease of the total Burgers vector below T^*, according to equation (1).

The dynamics of the transformation displays two characteristic features: it is abrupt and it is reversible. We believe that it is governed by the switching from a prenematic *non-isometric* elastic regime above T^* to the conventional *isometric* smectic behaviour below T^*. We use here the qualifiers 'isometric' and 'non-isometric' in the sense defined in (20) (see Appendix A). In the non-isometric elastic regime the distortions of the smectic layers relax mainly through the appearance of dislocations and curvature walls, at the expense of the equidistance and parallelism of the layers, whereas in the isometric regime there is rather a proliferation of FCDs, such that the curved layers remain equidistant and parallel in the largest possible volume of the

sample, which also implies that the density of kinks is minimised. It is reasonable to expect that the balance between dislocations and kinks on one hand, and FCDs on the other, depends on temperature, more exactly on the variation with T of the physical constants (see (7)). The *instability* which results from this competition depends also on the boundary conditions; in the present case, where the anchoring is strong and opposes the formation of ideal FCDs at the substrate, we expect that the transformation from an isometric regime with numerous small FCDs to a non-isometric regime with plenty of dislocations, happens at a rather low temperature T^*. The fact that the instability temperature is so well defined might be a result of the uniformity of the boundary conditions, which are dominated by the strong anchoring conditions.
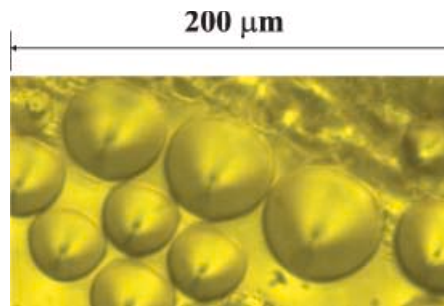

Figure 5. FCDs in thick free-standing films.

The same characteristics of abruptness and reversibility are also observed with the phenomenon of disappearance of the ellipses, described later in section 3.2, when the temperature increases; we
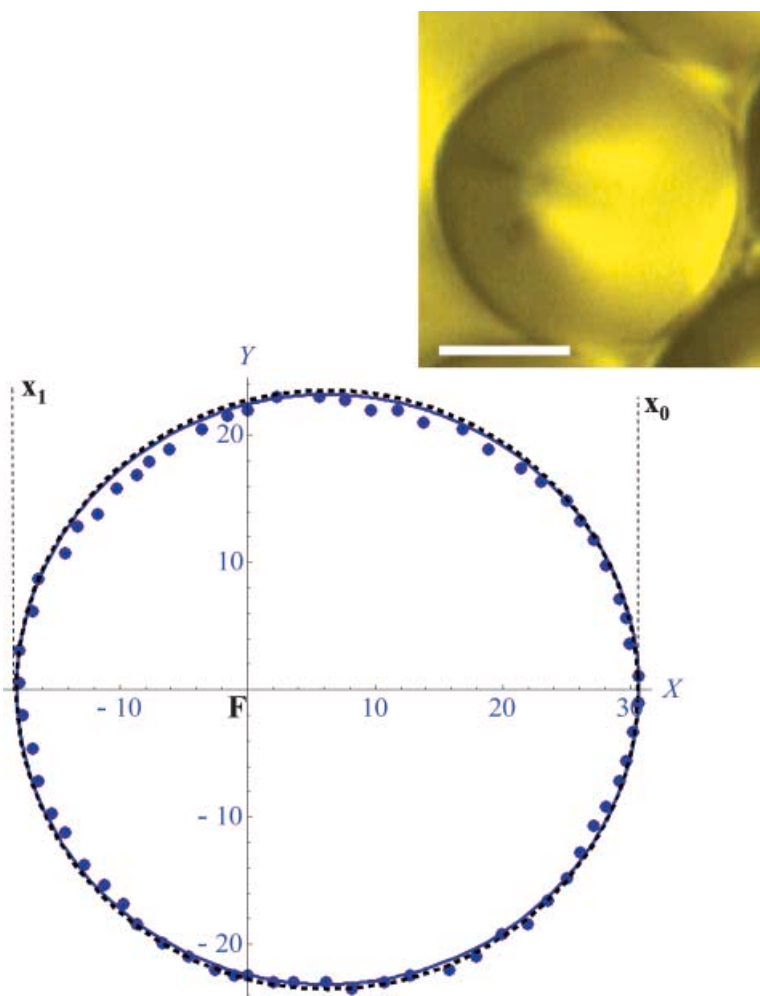
Figure 6. Best fits of the experimental ellipse (dots) belonging to a FCD (shown in the photograph above the plots, the scale bar is 20 μm) in thick free-standing smectic film by the Mouse model (equation (13), solid line) and by the ideal ellipse (equation (15), dashed line). As expected, the difference between the ideal ellipse and the mouse is small (<1 μm) and the ideal ellipse appears outside both the experimental and theoretical imperfect ellipses.

shall argue that they belong to the same type of instability.

2.3.   *Microscopic kinks; the mouse*

Deformed ellipses of the Mouse type (those with in-plane kinks) are obtained in free-standing films. A SmA drop is deposited and spread over a hole of a metallic collar with an internal diameter of 5 mm and thickness of 2 mm. After the relaxation of the smectic film, we obtain an ordinary free standing SmA film, which as a rule contains few smectic layers and which looks black between crossed polarisers. Then an additional drop of the same SmA is deposited at the centre of the free-standing film. This deposition has to be careful not to break the existing thin film. The immediate microscope observations reveal that the added material does not fall through the thin film. Instead the film serves as a substrate for the added material, which spreads towards the film periphery producing terraces and rows of FCDs (Figure 5). After several hours the film has a thickness profile varying from a few micrometres at its centre to several hundreds of micrometres at its periphery and is stable in time.

These large FCDs (from tens to several hundreds of micrometres in diameter) have never been documented before in free-standing films (except in our recent paper (7)). There are multiple advantages of this geometry. Although azimuthal anchoring conditions of the molecules on two surfaces of the film are homeotropic, hence azimuthally degenerate, the orientation of the FCDs is not random. Orientation, position and size of ellipses and hyperbolae are predetermined by the wedge character of the film periphery: (1) the ellipse planes are to be found within the midplane of the film; (2) the hyperbolae are pointed towards the direction of smaller film thickness; (3) the eccentricity e of the ellipses is non-zero and defined by the wedge angle ω of the film meniscus through the relation $e=\sin(\omega/2)$; (4) the FCDs are arranged in circular rows such that the size of their ellipses is roughly the same within a row and increases in the direction towards the film periphery; (5) owing to the curved profile of the meniscus surface, the FCD ellipse is expected to be distorted, first, because the wedge angle ω of the film and consequently the eccentricity of the ellipse and, second, because the thickness of the film and consequently the size of the ellipse have to be increasing
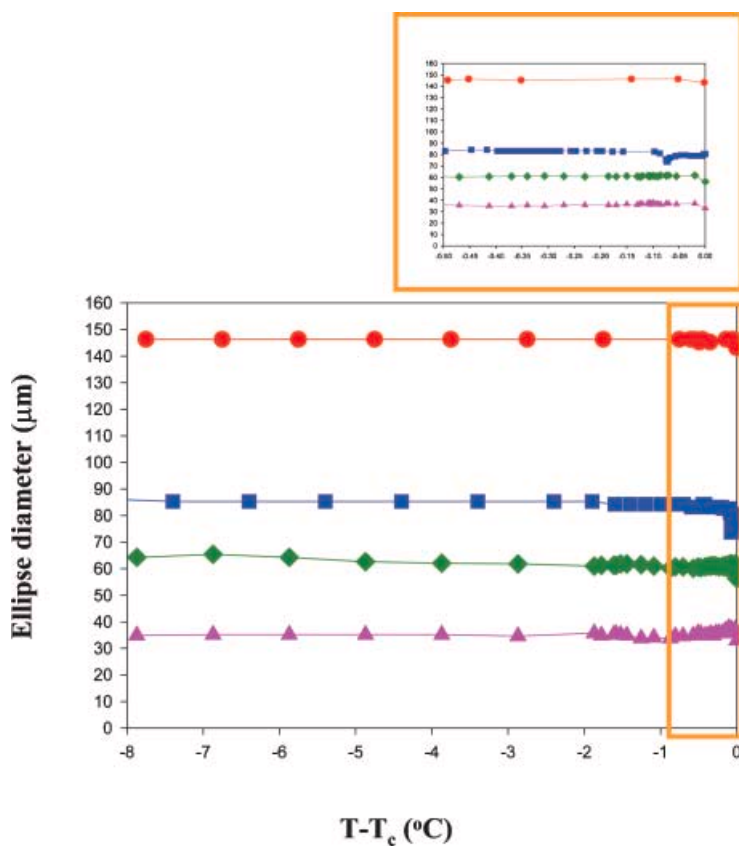

Figure 7. Temperature evolution of the FCDs size in 10CB in a broad temperature region; inset: near the transition to the isotropic phase.
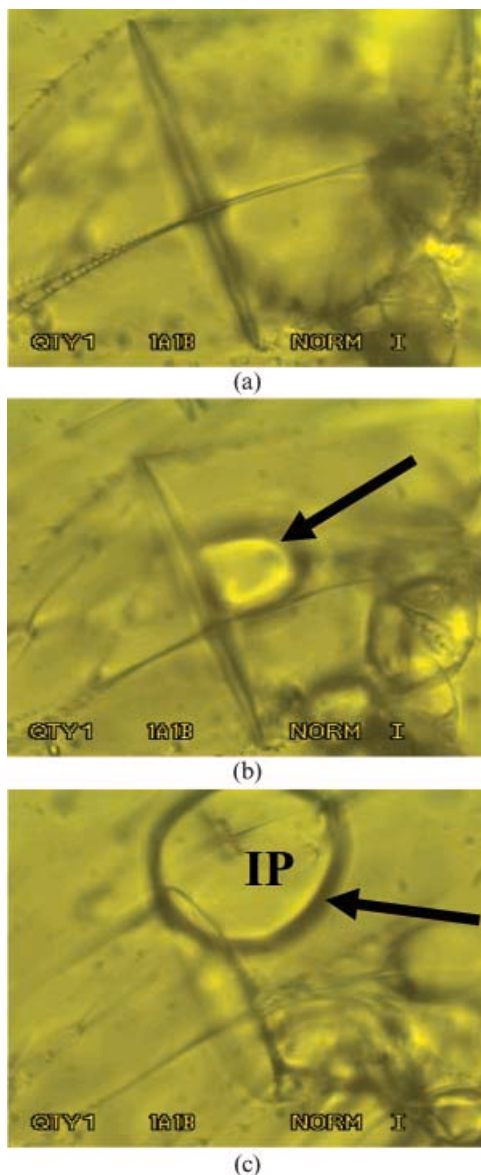
Figure 8. Observations of the temperature evolution of the FCD size in 10CB taken: (a) at 7.24°C below the SmA–ISO phase transition (upper photograph); (b), (c) at the temperature when the isotropic phase (shown by arrows) appears. The photographs correspond to the plot shown in Figure 7.

functions of the distance from the centre of the film. Owing to the specific shape of the ellipse, such a distorted FCD is called a *mouse*. A theoretical analysis of the mouse shape is developed in Appendix B see also the schematic drawings in our previous paper (*7*)). We have studied in detail several mice in various samples: an illustration of the results is given in Figure 6, which shows an experimentally observed shape (shown in the inset), and for comparison the shape predicted by the mouse model (equations (12), (14) and (15)) and the shape of the
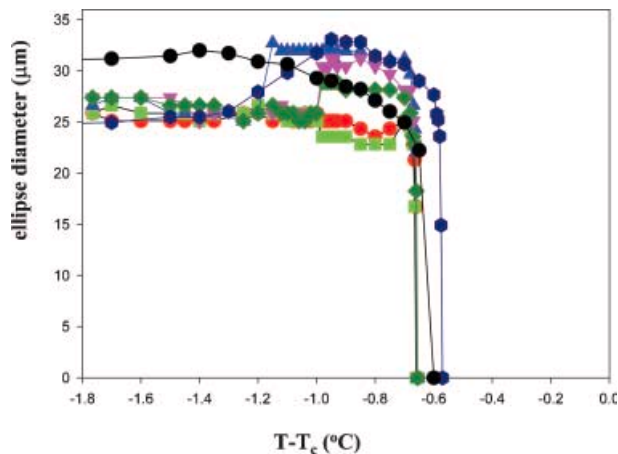

Figure 9. Temperature evolution of the FCDs size in 8CB.

corresponding ideal ellipses (equations (17)–(19)). As expected by the model, the ideal ellipse is outside the imperfect, experimental ellipse, at a distance which is in qualitative agreement with equation (21).

3. Size evolution of FCDs for nematogenic and non-nematogenic materials

3.1. *FCDs in a non-nematogenic smectic*

In the 10CB non-nematogenic material, the vast majority of FCDs do not suffer any visible change in size until the frontier with the isotropic phase comes in contact with the FCD. The measured temperature dependence of the FCD size is plotted in Figure 7. The photograph with a lopsided FCD in Figure 8 (a) corresponds to a temperature well below the transition temperature, while the two other photographs were taken at the temperature when the isotropic phase appears. Figure 8 (b) and (c) contain the interface between the SmA and isotropic phase (shown by an arrow). It is observed that the size of the FCD does not decrease essentially approaching the phase transition. When the interface touches the FCDs, the ellipse shrinks (Figure 8 (c), corresponding to $T–T_c=0$) and disappears. As shown in the next section, the situation is quite different for the nematogenic SmA.

3.2. *Temperature transformations of FCDs in thick free-standing films of nematogenic smectics*

3.2.1. *Heating*

The prenematic transformations of FCDs take place in a broad temperature region. In the nematogenic 8CB, 8OCB and 9CB materials there is a clearly visible pretransitional tendency to the disappearance of the FCDs. The temperature distance from the
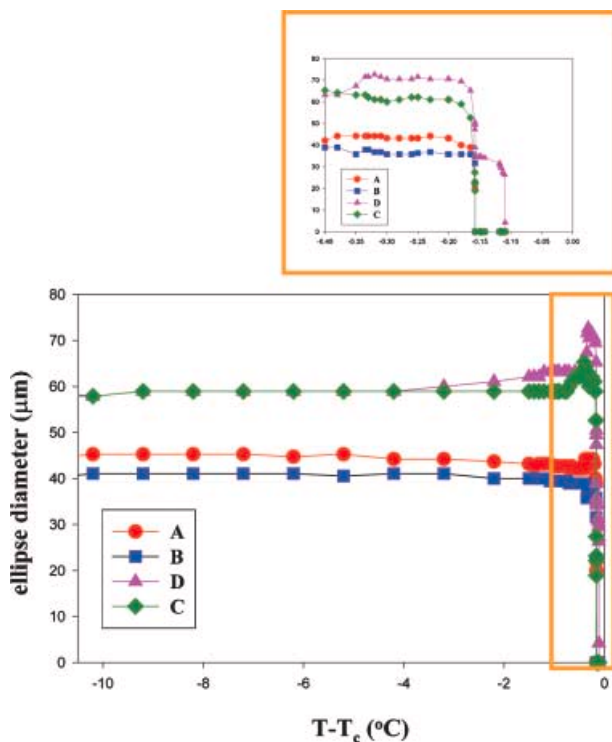
Figure 10. Temperature evolution of the FCDs size in 8OCB in a broad temperature region; inset: near the transition to the nematic phase. The corresponding modifications of the FCDs are illustrated in Figure 11.

phase transition, where a particular FCD disappears, depends on its size: smaller FCDs disappear at lower temperatures. Figures 9 and 10 show plots displaying the temperature behaviour of the FCD size (Figure 9 for 8CB and Figure 10 for 8OCB). Some of the graphs contain abrupt steps, which we think result from the textural transformations between the isometric and non-isometric elastic regimes evidenced in section 2.2.2. However, all the plots for nematogenic materials display pre-transitional shrinking of the ellipses, as is clearly seen in the vicinity of the phase transition, enlarged in the inset of Figure 10 (compare with the inset of Figure 7, where no such vanishing tendency is observed for a non-nematogenic SmA material).

The evolution of the ellipse size plotted in Figures 9 and 10 has a negligible time-dependent component. We checked this for the pretransition region in the immediate vicinity of the point at which later heating caused the ellipse to disappear. For example, the temperature was stabilised for 25 min at $0.005°C$ below the temperature at which the ellipse disappeared on later heating, and the photographs taken in the course of time during the temperature stabilisation do not reveal any changes in the size, while on further heating the ellipse disappears. We

have carefully checked the time stability of the ellipse size in all of the measured temperature ranges, stabilising at particular chosen temperatures and measuring the size in the course of time. The ellipse shrinks continuously when the temperature increases, and ceases to change when the temperature is stabilised, but only to some threshold size a_c for the longer ellipse diameter, after which the ellipse disappears suddenly, even if the temperature does not increase further or even if the temperature decreases. This threshold size of the ellipse was roughly the same for all examined ellipses in the studied nematogenic SmA materials and is about $a_c \approx 10\,\mu m$. The FCDs with a diameter smaller than about $10\,\mu m$ are not stable and collapse. Continuous shrinking of the ellipse is accompanied by an increase in the eccentricity of the ellipse (see Figures 11 (a)–(d) and 12).

3.2.2. Temperature cycling

To check whether the pretransition changes of the ellipse size are reversible, we have performed temperature cycling. The temperature was stabilised for about 10 min at point 1 in Figure 13 (cycle *A*), which is close to the nematic transition. Then it was gradually increased to point 2. Measurements of the ellipse size (dots in the cycle *A*, Figure 13) at temperatures between points 1 and 2 show that it decreases on heating. Then the sample was cooled back to the temperature corresponding to the point 3. Measurements of the ellipse size (full squares), at intermediate temperatures between points 2 and 3, display an increase of ellipse size but the ellipse does not recover its previous size even at the temperature corresponding to point 3, which is significantly lower than that for point 1. The temperature modifications of the ellipse size in the cycles that follow are also plotted in Figure 13.

At least three conclusions can be drawn from the cycling procedure described above. First, on heating approaching the nematic phase transition, the ellipse size decreases, while on back cooling it increases. Second, the temperature evolution of the ellipses is reversible, but only partially: the ellipse size does not recover but remains smaller when after the heating the sample is cooled back to the starting temperature. The partial reversibility of the temperature evolution of the FCDs suggests that at a given stabilised temperature there is equilibrium between the area occupied by FCDs and by dislocations. When the sample is heated, the area occupied by free dislocations (those not attached to the ellipses) increases at the expense of the decrease of the sizes of the FCDs. On back cooling the FCDs expand at the expense of the area occupied by free dislocations. The
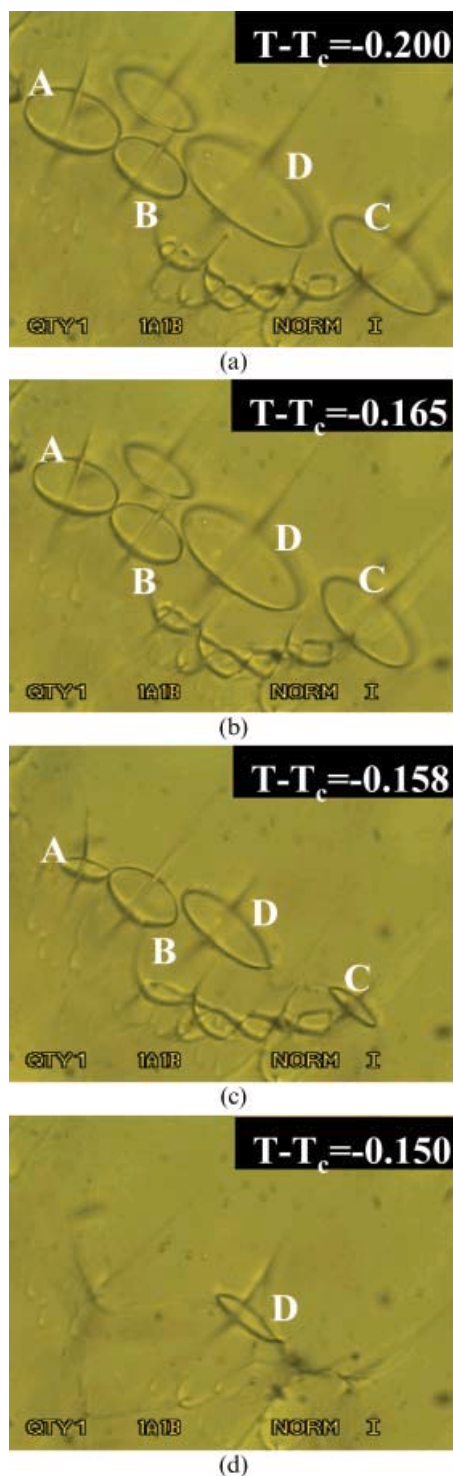
Figure 11. (a)–(d) Microscope photographs illustrating the temperature evolution of the FCDs in 8OCB. The notation A–D corresponds to the dependencies shown in Figure 10.
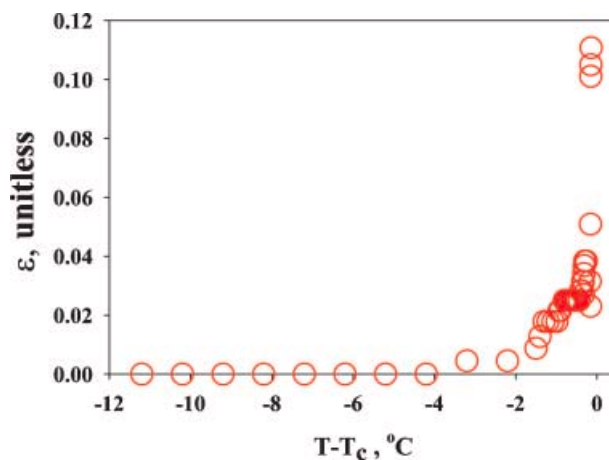

Figure 12. Temperature variation $\varepsilon(\Delta T)$ of the eccentricity measured for the ellipse D (see Figure 11). Here $\varepsilon(\Delta T) = (e_0 - e(\Delta T))/e_0$, $\Delta T = T - T_c$ is the distance from the nematic phase transition, e_0 is the eccentricity value measured far from the nematic phase transition, $e(\Delta T)$ is the eccentricity value measured at a given ΔT.

cooling is only partially reversible. In other words, the partial reversibilizty of the temperature evolution of the FCDs implies that the shrinking of the ellipse on heating is energetically easier than its back expanding on further cooling. Indeed the shrinking of the ellipse is accompanied by the emission of the dislocations by their separation from the ellipse, while the reverse process of ellipse expanding requires the attachment of the dislocations to the ellipse. However, the dislocations are usually pinned by their ends on the sample interfaces or on other defects. The latter will hinder the expansion of the ellipse. Third, small ellipses with a diameter smaller than 10 μm are unstable: they collapse and disappear.

3.2.3. The nature of the textural transformation

The transformation described in this section is certainly not a phase transition, since it depends on the size of the ellipses; it is rather an *instability* strongly dependent on the boundary conditions to which the ellipse sizes indeed contribute. We believe that this instability is the same as that related to the textural transformation of section 2.2.2; it is also related to the modifications of a tilt grain boundary. However, the boundary conditions are completely different; in the present case, the ellipses are hardly in contact and their eccentricity, $e = \sin(\omega/2)$ is rather large, which implies that in the description of Kleman and Lavrentovich (*18*) (see Appendix A) the grain boundary structure is close to a curvature wall. It is difficult to decide whether the (large) interstitial regions between the ellipses are still filled with dislocations (as in section 2.2.2) or are already

expanding of the FCDs is most probably accompanied by the attachment of some of the free dislocations to the ellipse. It is plausible that due to limited mobility of the dislocations, the expanding of the FCDs on

Cycle A : (1 → 2 → 3)

Cycle B: (3 → 4 → 5)
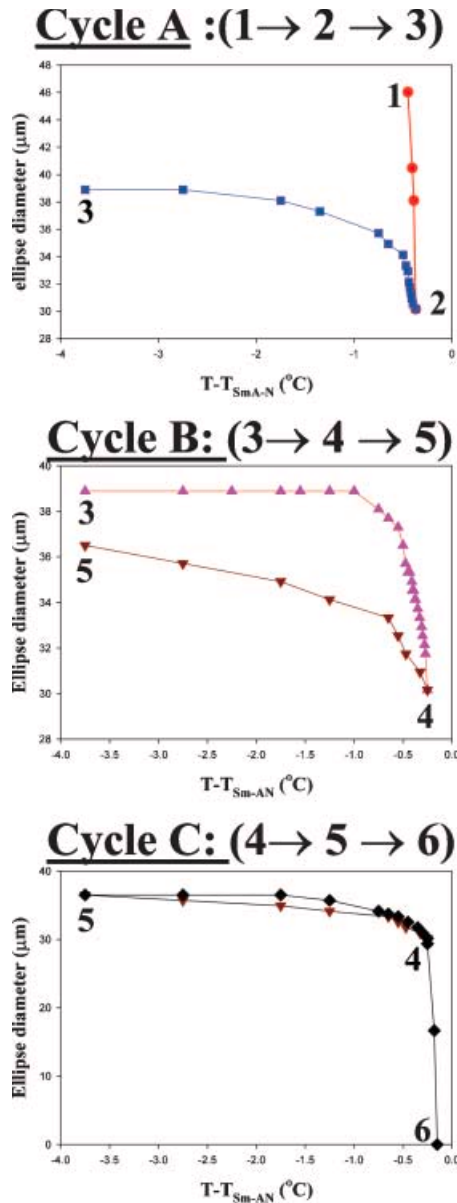

Cycle C: (4 → 5 → 6)

Figure 13. Temperature cycles of the FCD evolution. Cycle A: the temperature was stabilised for about 10 min at point 1, increased to point 2 (dots) and then decreased to the temperature corresponding to point 3 (solid squares). Cycle B: the temperature increases and the ellipse size (upward triangles) decreases between points 3 and 4. At point 4 the temperature was stabilised for a few minutes and then again decreased to point 5 (downward triangles). Cycle C: heating (rhombuses) from point 5 to point 6, where the ellipse disappears. For comparison, the branch '4→5' (downward triangles) of the previous cycle B is also shown in cycle C.

Figure 14. Schematic presentation of the profile of the free-standing film containing a FCD in its midplane with the notation used in Appendix B: ρ is the curvature radius of the film meniscus; η is the x-coordinate of the centre of the film; F is the origin of the coordinate system located in the focus of the ellipse; the ellipse is in the XY-plane; ω is the misorientation angle of a grain boundary located in the midplane of the film; the eccentricity of the ellipse is $e=\sin\omega/2=(x-\eta)/\rho$; x_0 and x_1 are x-coordinates of the two opposite extremities of the ellipse on the X-axis.

curvature wall regions. However, there is no doubt that a curvature wall is more non-isometric (in the sense of section 2.2.2) than a tiling of the grain boundary by ellipses and the FCDs they belong to. The eccentricity of the ellipses increases with
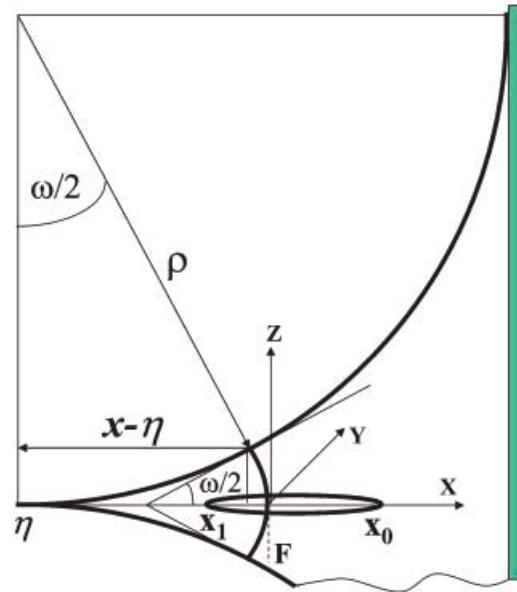
temperature, which also indicates a transformation towards curvature walls in the prenematic region.

This modification of the ellipse eccentricities requires, of course, a modification of the kink distribution, whose Burgers vector density measured along the major axis is $db_{disl}=2e\ dx$ (equation (7), Appendix B); the total Burgers vector attached to an ellipse is $4e\ a=4c$. The notion of kink, which has been developed for the dislocation–disclination interaction, is topological, and it does not matter whether the objects attached to the ellipse are dislocations, or whether a curvature wall extends between ellipses, to use the language of dislocations. However, the local distribution of strains at the attachment, or along the topological object in movement in order to change the equivalent total Burgers vector, depends on the nature of the topological object, dislocation of fragment of a curvature wall. However, this is a question that we do not consider here.

4. Conclusion

We have documented polarisation microscopy textures of imperfect FCDs. In real samples the FCDs can contain in-plane or out-of-plane *kinks* (FCDs of the mouse or turtle type, respectively). The mouse

shape has been fitted by proposed theoretical equations, which are in good agreement with the experimental observations.

Two types of smectics, namely nematogenic and non-nematogenic have shown very different temperature evolution of the FCD size. For nematogenic smectics the FCDs decrease in size and then disappear while still in the smectic phase on heating in the region at some distance from the temperature of the nematic phase transition. Temperature cycling displays partial reversibility of the FCD size. When on heating a FCD becomes smaller than about 10 μm in diameter, it collapses, vanishing even if the temperature is stabilised or decreased. For the non-nematogenic smectics, the FCDs do not change their size until the interface with the isotropic phase touches the FCD. In the nematogenic smectic films deposited on unidirectionally rubbed substrate we have observed a reversible sudden temperature induced transformation of the FCD texture.

We believe that the observed temperature transformations of the FCDs are due to variations of the material constants, which are large enough to cause *isometric* to *non-isometric* instabilities. In the so-called isometric regime (at lower temperatures), the parallelism of a vast majority of the layers (but not all, see Appendix A), characteristic of a smectic phase in its ground state, is conserved; in the non-isometric regime (closer to the nematic phase) the constraint of parallelism is somewhat relaxed and dislocations or curvature walls are numerous. The transition between the two regimes is controlled by kinks. The extent of the '*prenematic*' region, where non-isometry is predominant, depends on boundary conditions; this region is high in temperature. A careful investigation of the magnitude of the material constants in this region could be of interest.

References

(1) Friedel J. *Dislocations*; Pergamon Press: London, 1964.
(2) Allain M. *Défauts thermodynamiques dans une phase lamellaire d'un système non-ionique*; PhD thesis, Université de Paris-Sud, Orsay, 1987.
(3) Blanc C.; Zuodar N.; Lelidis I.; Kleman M.; Martin J.-L. *Phys. Rev. E* **2004**, *69*, 011705.
(4) Kleman M.; Lavrentovich O.D. *Soft Matter Physics. An Introduction*; Springer: New York, 2003.
(5) Kleman M.; Lavrentovich O.D.; Nastishin Yu.A. *Dislocations and Disclinations in Mesomorphic Phases*; Dislocations in Solids 12; ed. by Nabarro F.R.N and Hirth J.P. (Eds), pp. 147–271, Elsevier, 2004.
(6) Friedel G.; Grandjean F. *Bull. Soc. Fr. Minér.* **1910**, *33*, 192.
(7) Kleman M.; Meyer C.; Nastishin Yu.A. *Philos. Mag.* **2006**, *86*, 4439.
(8) Meyer C.; Nastishin Yu.A.; Kleman M. Mol. Cryst. Liq. Cryst. **2007**, *477*, 537–547.
(9) Friedel J.; Kleman M. *J. Phys. (Paris)* **1969**, *30*, 43.
(10) Kleman M.; Friedel J. *Rev. Mod. Phys.* **2008**, *80*, 61.
(11) Meyer C.; Kleman M. *Mol. Cryst. Liq. Cryst.* **2005**, *437*, 1355–1363.
(12) Friedel G. *Ann. Phys. (Paris)* **1922**, *18*, 273.
(13) Bouligand Y. *J. Phys. (Paris)* **1972**, *33*, 525.
(14) Demus D.; Richter L. *Textures of Liquid Crystals*; VEB Deutscher Verlag fur Grundstoffindustrie: Leipzig, 1980.
(15) Nastishin Yu.A.; Polak R.D.; Shiyanovskii S.V.; Bodnar V.H.; Lavrentovich O.D. *J. Appl. Phys.* **1999**, *86*, 4199.
(16) Qian T.; Zhuang X.; Shen Y.R. *Phys. Rev. E* **1999**, *59*, 1873.
(17) Pishnyak O.P.; Nastishin Yu.A.; Lavrentovich O.D. *Phys. Rev. Lett.* **2004**, *93*, 109401.
(18) Kleman M.; Lavrentovich O.D. *Eur. Phys. J. E* **2000**, *2*, 47–57.
(19) Williams C.; Kleman M. *J. Phys. (Paris)* **1975**, *36*, 315.
(20) Achard M.-F.; Kleman M.; Nastishin Yu.A.; Nguyen H.T. *Eur. Phys. J. E* **2005**, *16*, 37.
(21) Bidaux R.; Boccara N.; Sarma G.; De Sèze L.; De Gennes P.G.; Parodi O. *J. Phys. (Paris)* **1973**, *34*, 661.
(22) Oswald P.; Lejcek L. *Eur. Phys. J. E* **2006**, *19*, 441.
(23) Geminard J.-C.; Holyst R.; Oswald P. *Phys. Rev. Lett.* **1997**, *78*, 1924.

Appendix A. Isometric and non-isometric deformations

We define isometric deformations as those that conserve the parallelism and the distances (between layers in smectic phases and between columns in columnar phases); they are commonplace in LCs. Isometric deformed textures display specific geometric features; also the order parameter singularities which respect to isometry can extend over large, macroscopic, distances, for example, cofocal conics in smectics, developable domains in columnar phases (*4–6*). The observation of defects and textures in the recently discovered liquid crystalline phases of bent-core molecules (banana shaped) has considerably enlarged the scope of possible isometric distortions, because some of these phases show simultaneously smectic, columnar ordering and macroscopic chirality (*20*).

Isometric domains do not tile space, so there are always non-isometric defects (such as dislocations or curvature walls) remaining in the interstices left between domains in contact. The question is, therefore, what is the typical size of the interstices or, in other words, what is the size of the smallest possible isometric domains. In SmAs this discriminating length is $\lambda = \sqrt{K/B}$, where K and B are elastic moduli for the curvature and strain deformations, respectively. Bidaux et al. (*21*) have indeed shown

that in a set of toric FCDs, with all of the disclination circles belonging to the same plane where they form an Apollonian tiling, the smallest circle diameters scale as λ.

The Apollonian tiling is a very peculiar FCD tiling; it constructs a grain boundary between two smectic grains that have the same orientation, the misorientation $\omega = 0$. Most often, FCDs form tilt grain boundaries when packing; all of the ellipses belong to the grain boundary, have the same eccentricity $e = \sin\omega/2$ and are in contact in this boundary. The angle ω measures the misorientation between layers perpendicular to the common asymptotic directions of the cofocal hyperbolas. The size and the nature of the interstices depends on λ, as already indicated, but also on ω (see (*18*)). For a very large $\omega \simeq \pi$, the layers curve smoothly from one direction to the other, the grain boundary is a curvature wall; thus, when approaching $\omega = \pi$, the interstices tend to become macroscopic. For a small $\omega \simeq 0$, the grain boundary is accommodated by a set of parallel edge dislocations, in the manner of a classical tilt boundary; thus, when approaching $\omega = 0$, the interstices also tend to become macroscopic. We speak of a non-isometric regime when such macroscopic regions, curvature walls or classical tilt boundaries appear. For all other misorientations, in fact for most of the interval $0 < \omega < \pi$, the grain boundary is made of FCD ellipses, with dislocations between the ellipses, extending from one ellipse to the next in small interstices. This is the isometric regime.

Appendix B. The mouse

B.1.   *The imperfect ellipse*

Let us consider a FCD with the ellipse located in the middle plane of the symmetrical free standing SmA film (Figure 14).

The equation of an ideal ellipse in polar coordinates (r, ϕ) is

$$r = \frac{p}{1 - e \cos \phi} \qquad (3)$$

where $p = b^2/a$ and e denote the parameter and the eccentricity of the ellipse, respectively; a is the semi-major axis and b is the semi-minor axis. The origin of the coordinates is taken at the left focus of the ellipse, which is the physical focus, located closer to the centre of the film than the other focus. The x-axis is chosen directed towards the film periphery. The size of the ellipse depends on the thickness of the film, but we shall not consider this question here.

Because of the curved meniscus of the film profile, the thickness d and the wedge angle ω of the film are functions of the x-coordinate and, thus, $p(x)$ and $e(x)$ are also functions of the x-coordinate (or the angle ϕ). Hence,

$$r = \frac{p(\phi)}{1 - e(\phi)\cos \phi}. \qquad (4)$$

Such deformed ellipses are called mice (see (*7*)). The smectic layers are no longer strictly parallel, but we make the reasonable assumption that they intersect the plane of the ellipse, inside it, along concentric circles centred at the focus of the ellipse; they remain parallel in this region. Calculating the differential of equation (2), we obtain

$$\frac{dr}{r} = \frac{dp}{p} + \frac{\cos \phi \, de}{1 - e \cos \phi} - \frac{e \sin \phi \, d\phi}{1 - e \cos \phi}. \qquad (5)$$

For an ideal ellipse:

$$dr = e \, dx. \qquad (6)$$

As shown in (*7*), the curved ellipse disclination, which is not a wedge disclination, has to carry a density of kinks at the layer scale, even in the ideal state. A density of dislocations is attached to those kinks, the Burgers vectors of which are perpendicular to the plane of the ellipse and can be written as

$$db_{\text{disl}} = 2e \, dx, \qquad (7)$$

in agreement with Figure 1. In fact, this density is made of quantised dislocations of Burgers vectors multiples of $2d_0$, d_0 being the layer repeat distance; each kink carries a Burgers vector $db_{\text{disl}} = 2d_0$. Indeed, according to equations (6) and (7), we have $db_{\text{disl}} = 2dr$; since the layers are falling perpendicular to the plane of the ellipse. With $dr = d_0$, this yields $db_{\text{disl}} = 2d_0$.

Making the hypothesis (which is exact without approximation in the case of an ideal ellipse (6)) that

$$dr \approx e \, dx \qquad (8)$$

one can rewrite equation (8) in the form

$$dr = \frac{-p(e \sin \phi)}{(1 - e \cos \phi)^2} \, d\phi. \qquad (9)$$

Equations (6) and (7) turn equation (5) into

$$\frac{dp}{de} + x = 0. \qquad (10)$$

The integration of equation (10) leads to

$$p = p_0 - \int_{x_0}^{x} x \frac{de}{dx} dx, \qquad (11)$$

where $p(\phi=0)=p(x_0)=p_0$ and $p(\phi=\pi)=p(x_1)=p_1$. The coordinates of the two apices M_0, $\phi=0$ and M_1, $\phi=\pi$ of the ellipse x_0 and x_1 are given by

$$x_0 = x(\phi=0) = r_{\phi=0} = \frac{p_0}{1-e_0} > 0 \quad \text{and}$$

$$x_1 = x(\phi=\pi) = -r_{\phi=\pi} = -\frac{p_1}{1+e_1} < 0.$$

Figure 14 represents the shape of the profile (see (22) for a comparable situation). Owing to the presence of terraces, the ellipses are deformed and appear to be more similar than mice; the semi-major axis is denoted by a, ω is the grain boundary angle, d is the sample thickness and η denotes the negative origin of the film.

We choose a simple profile of the meniscus obeying (23):

$$e = \frac{x-\eta}{\rho}, \qquad (12)$$

where ρ is the curvature radius of the freely suspended film (see Figure 14).

In polar coordinates, $x = r\cos\phi = (p\cos\phi)/(1-e\cos\phi)$, which can be rewritten as

$$\phi = \arccos \frac{x}{p+e\,x}. \qquad (13)$$

Therefore, one has

$$y = r\sin\phi = \sqrt{(e^2-1)x^2 + 2e\,px + p^2}. \qquad (14)$$

Keeping in mind the expression of the eccentricity equation (12), the expression of the parameter $p(\phi)$ reads as follows:

$$p = p_0 - \frac{1}{2\rho}(x^2 - x_0^2). \qquad (15)$$

B.2. *The ideal ellipse versus the imperfect ellipse*

Let a^*, b^*, c^*, $e^*=c^*/a^*$, $p^*=b^{*2}/a^*$ denote the geometrical parameters relating to an ideal ellipse $r^*=p^*/(1-e^*\cos\phi^*)$, which we wish to compare with the imperfect ellipse above. We define such an ideal ellipse as the ellipse with the same apices as the imperfect ellipse, namely x_0, x_1, and the same focus at $x=0$. Hence, the same polar coordinates at the same

origin. In these definitions the choice of the focus has a clear physical content: whichever FCD is built from this ideal ellipse, the smectic layers intersect the plane of the ellipse along the same circles centred at this focus; this was in fact also the central geometrical property of our construction of the imperfect ellipse.

We then have

$$x_0 = \frac{p^*}{1-e^*} = \frac{p_0}{1-e_0}, \quad -x_1 = \frac{p^*}{1+e^*} = \frac{p_1}{1+e_1}, \qquad (16)$$

from which relations we obtain

$$e^* = \frac{x_0+x_1}{x_0-x_1}, \quad p^* = \frac{-2x_0x_1}{x_0-x_1}. \qquad (17)$$

It suffices to compare the ordinates of the imperfect ellipse and of the ideal ellipse for the value of $x=0$, in order to have some feeling how the experimental 'ellipse' differs from an ideal ellipse. We have

$$y^*(0) = p^*, \quad y(0) = p_0 + \frac{1}{2\rho}x_0^2 \equiv p_1 + \frac{1}{2\rho}x_1^2. \qquad (18)$$

We can express these quantities as a function of half the major axis $a = a^* = \frac{1}{2}(x_0-x_1)$ and of the abscissa of the centre of the ellipses $x_C = x_C^* = \frac{1}{2}(x_0+x_1) = c^*$. We obtain

$$p^* = \frac{b^{*2}}{a}, \quad p(x=0) = \frac{1}{2}\left(p_0 + \frac{1}{2\rho}x_0^2 + p_1 + \frac{1}{2\rho}x_1^2\right)$$

$$= a + \frac{\eta}{\rho}c^* - \frac{1}{2\rho}\left(a^2 + c^{*2}\right), \qquad (19)$$

i.e.

$$\delta = y(x=0) - y^*(x=0)$$

$$= \frac{\eta}{\rho}c^* - \frac{a^2}{2\rho} + c^{*2}\left(\frac{1}{a} - \frac{1}{2\rho}\right). \qquad (20)$$

The first two terms are negative and the third term is positive. The difficulty of the sign of δ may be solved by noticing that since

$$p_0 + \frac{1}{2\rho}x_0^2 = p_1 + \frac{1}{2\rho}x_1^2,$$

we also have

$$c^*\left(\frac{1}{a} - \frac{1}{\rho}\right) = -\frac{\eta}{\rho},$$

hence, after some algebra:

$$\delta = -\frac{b^{*2}}{2\rho} < 0. \qquad (21)$$

Substituting typical values for the ellipse half-diameter $b^*=25\,\mu$m and for the curvature radius $\rho=10^3\,\mu$m, we find that the deviation of the deformed ellipse from the ideal ellipse is expected to be quite small $|\delta|\sim0.3\,\mu$m. Of course, the larger the radius of curvature, the smaller the quantity $|\delta|$. Such a small value cannot be measured with an optical microscope. However, according to equation (20), δ is negative indicating that the ideal ellipse is expected to be *outside* the imperfect ellipse and, hence, the mouse model can be qualitatively tested by fitting the experimental shape of a FCD ellipse by equations (13) and (15) for the ideal ellipse (dashed line in Figure 6) and mouse (solid line), respectively, and comparing their positions with respect to each other and with respect to the experimental ellipse (dots). This expectation of the model has been observed for three ellipses belonging to two different samples.